Human Molecular Genetics, 2013, Vol. 22, No. 20 **4148–4163**
doi:10.1093/hmg/ddt263
Advance Access published on June 6, 2013

Type of uromodulin mutation and allelic status influence onset and severity of uromodulin-associated kidney disease in mice

Elisabeth Kemter[1,*], Petra Prueckl[1], Stefanie Sklenak[1], Birgit Rathkolb[1,2], Felix A. Habermann[3], Wolfgang Hans[2], Valérie Gailus-Durner[2], Helmut Fuchs[2], Martin Hrabě de Angelis[2,5], Eckhard Wolf[1], Bernhard Aigner[1] and Ruediger Wanke[4]

[1]Chair for Molecular Animal Breeding and Biotechnology, Gene Center, Ludwig-Maximilians-Universitaet (LMU) Muenchen, Munich 81377, Germany, [2]German Mouse Clinic, Institute of Experimental Genetics, Helmholtz Zentrum Muenchen, Neuherberg 85764, Germany, [3]Chair for Veterinary Anatomy, Histology and Embryology, Department of Veterinary Sciences and [4]Institute of Veterinary Pathology, Center for Clinical Veterinary Medicine, Ludwig-Maximilians-Universitaet (LMU) Muenchen, Munich 80539, Germany and [5]Chair of Experimental Genetics, Center of Life and Food Sciences Weihenstephan, Technische Universitaet Muenchen, Freising-Weihenstephan 85350, Germany

Received April 24, 2013; Revised May 30, 2013; Accepted June 1, 2013

Uromodulin-associated kidney disease (UAKD) is a dominant heritable renal disease in humans which is caused by mutations in the uromodulin (*UMOD)* gene and characterized by heterogeneous clinical appearance. To get insights into possible causes of this heterogeneity of UAKD, we describe the new mutant mouse line *Umod*^{C93F}, leading to disruption of a putative disulfide bond which is also absent in a known human *UMOD* mutation, and compare the phenotype of this new mouse line with the recently published mouse line *Umod*^{A227T}. In both mutant mouse lines, which were both bred on the C3H background, the *Umod* mutations cause a gain-of-toxic function due to a maturation defect of the mutant uromodulin leading to a dysfunction of thick ascending limb of Henle's loop (TALH) cells of the kidney. *Umod* mutant mice exhibit increased plasma urea and Cystatin levels, impaired urinary concentration ability, reduced fractional excretion of uric acid and nephropathological alterations including uromodulin retention in TALH cells, interstitial fibrosis and inflammatory cell infiltrations, tubular atrophy and occasional glomerulo- und tubulocystic changes, a phenotype highly similar to UAKD in humans. The maturation defect of mutant uromodulin leads to the accumulation of immature uromodulin in the endoplasmic reticulum (ER) and to ER hyperplasia. Further, this study was able to demonstrate for the first time *in vivo* that the severity of the uromodulin maturation defect as well as onset and speed of progression of renal dysfunction and morphological alterations are strongly dependent on the particular *Umod* mutation itself and the zygosity status.

INTRODUCTION

Uromodulin-associated kidney disease (UAKD) is an autosomal-dominant hereditary and slowly progressive disorder caused by mutations of the uromodulin (*UMOD*) gene (1,2). UAKD summarizes several clinically defined diseases including medullary cystic kidney disease type 2 (MCKD2; OMIM #603860), familial juvenile hyperuricemic nephropathy (FJHN; OMIM #162000) and glomerulocystic kidney disease (GCKD; OMIM #609886). To date, more than 70 distinct UAKD-causing *UMOD* mutations are known (3–5). The clinical manifestations of UAKD are hypouricosuric hyperuricemia, gout, mild defects in urine concentrating ability and it has a variable rate of disease progression between individuals leading to renal failure (1,6,7). Tubulointerstitial fibrosis with moderate inflammatory cell infiltration, tubular atrophy and cysts were

*To whom correspondence should be addressed at: Chair for Molecular Animal Breeding and Biotechnology, Gene Center, Ludwig-Maximilians-Universitaet (LMU) Muenchen, Feodor-Lynen Str. 25, D-81377 Munich, Germany. Tel: +49 89218076802; Fax: +49 89218076849; Email: kemter@lmb.uni-muenchen.de

described as histological alterations of the kidneys of UAKD patients (4,8). Hyperuricemia is mostly the first clinical sign which is diagnosed in UAKD patients, however, it is manifested in most but not all UAKD patients (7). Inconstant clinical signs, diagnosed in some patients, are small kidneys probably due to progressive renal scarring, hypertension and, in one report of patients harboring an *UMOD* indel-mutation, upper urinary tract infection (5,9,10). Further, time-point of first diagnosis of UAKD and rate of decline of kidney function varies within and between affected families and, comparing 37 distinct *UMOD* mutations in UAKD patients belonging to 45 families, no correlation of severity of clinical symptoms and the corresponding causative *UMOD* mutation could be drawn (2,11).

Uromodulin was originally identified over 60 years ago as Tamm-Horsfall glycoprotein and is the most abundant protein in mammalian urine (12,13). It is synthesized exclusively and abundantly in the cells of the thick ascending limb of Henle's loop (TALH) without macula densa cells and of the early part of the distal convoluted tubule (14). Human mature uromodulin glycoprotein consists of 590 amino acids with 48 cysteines and eight potential N-linked glycosylation sites (13), of which seven appear to be occupied (15). It is anchored at the luminal membrane of TALH cells by a GPI-anchor and is released in the urine by proteolytic cleavage (16). Haploinsufficiency of uromodulin does not cause UAKD as demonstrated by *Umod* knockout mice (17,18). All but four (in-frame deletions) UAKD-causing *UMOD* mutations are missense changes predicted to cause protein misfolding (3,4). Mutant uromodulin proteins show delayed ER to Golgi trafficking (6,19). The recently characterized mutant mouse line $Umod^{A227T}$ enabled the classification of an uromodulin mutation as gain of toxic function mutation causing TALH dysfunction and clinical signs (20).

In various genome-wide association (GWAS) studies, common allelic *UMOD* variants were identified to be associated with increased risk for complex traits such as chronic kidney disease, altered plasma uric acid levels or kidney stones (21–23). Thus, common allelic *UMOD* promoter variants influence *UMOD* expression, leading to altered plasma uric acid levels (24). As reviewed by Rampoldi *et al*. (4), the common allelic *UMOD* variants detected in GWAS studies lead to increased urinary uromodulin levels and the pathophysiology of this is so far nearly unknown. In contrast, rare allelic *UMOD* variants which affect amino acid sequence lead to UAKD associated with uromodulin trafficking defect and decreased urinary uromodulin levels.

We recently described the UAKD phenotype of the mutant mouse line $Umod^{A227T}$ (20). The aim of the present study was to characterize a second chemically induced *Umod* mutant mouse line called $Umod^{C93F}$ and to analyze the effects of different *Umod* mutations ($Umod^{A227T}$ and $Umod^{C93F}$) and of allelic status of *Umod* mutant mice on onset, severity and progression of clinical phenotype and morphological kidney alterations.

RESULTS

Establishment of the mutant mouse line $Umod^{C93F}$

The generation of the chemically induced mutant mouse line UREHD1 within the Munich ENU mouse mutagenesis project was described previously (25). This mouse line exhibited increased plasma urea levels, which was heritable in an autosomal-dominant manner. Linkage analyses revealed linkage of the causative mutation to a defined single chromosomal site on chromosome 7 between 116.8 (D7Mit40) and 125.3 Mb (D7Mit68). The strongest linkage of the causative mutation was observed with the polymorphic marker D7Mit238 (119.1 Mb). The probability of the existence of confounding non-segregating mutations in the detected chromosomal region is $P < 0.001$ (26). Sequence analysis of *Umod* cDNA, whose gene is located at 119.5 Mb on chromosome 7, revealed a G→T transversion in exon 3 at nt 470 (NM_009470) (Supplementary Material, Fig. S1A). Genotypic differentiation was enabled by allele-specific PCR reactions (Supplementary Material, Fig. S1B). Mating of heterozygotes to wild-type mice and of heterozygous mutant mice showed the expected Mendelian pattern of inheritance of the mutation in the offspring.

The identified mutation leads to an amino acid substitution of cysteine to phenylalanine at position 93 of uromodulin. Thus, the nephropathic line was named Munich $Umod^{C93F}$ mutant mouse line. C93 is assumed to form a disulfide bond with C105 (Supplementary Material, Fig. S1C). Hence, the disulfide bond C93–C105 is absent in mutant uromodulin, as it is also the case in the human uromodulin protein derived from the mutant allele $UMOD^{C106Y}$.

Clinical and clinical-chemical data of adult $Umod^{C93F}$ mutant mice

Detailed clinical and clinical-chemical analyses were carried out on $Umod^{C93F}$ mutant mouse line. In 8-month-old heterozygous $Umod^{C93F}$ mutants, plasma urea levels were increased 2-fold in both genders compared with their wild-type littermate controls (Table 1). Mutants also exhibited significantly increased plasma creatinine levels. A moderate but significant increase of potassium, calcium and alkaline phosphatase was detected in mutants of both genders. In contrast, mutants of both genders exhibited a significant decrease of triglycerides, ferritin and transferrin. Cholesterol was significantly decreased in male heterozygotes, and iron as well as inorganic phosphorus was significantly decreased in female heterozygotes. Plasma magnesium levels determined in 9-month-old mice were not significantly different between male (0.64 ± 0.06 mmol/l) and female (0.72 ± 0.12 mmol/l) heterozygous $Umod^{C93F}$ mutants versus wild-type littermates (male: 0.68 ± 0.07 mmol/l; female: 0.73 ± 0.05 mmol/l).

In 9-month-old heterozygous $Umod^{C93F}$ mutant mice, a 1.7- to 2.1-fold increase in daily urine volume and a significant decrease in urine osmolality were detected compared with wild-type controls (Table 2; Supplementary Material, Fig. S2A and B). Daily urinary excretion of several solutes was significantly different in mutants compared with wild-type controls. Thus, urine-to-plasma concentration ratios (U/P) for sodium, potassium and chloride were significantly reduced, whereas 24 h excretion and fractional excretion (FE) of these solutes were increased. All parameters were altered significantly except for 24 h excretion of sodium ($P = 0.11$) and chloride ($P = 0.06$) in heterozygous mutant males. A 3-fold increased 24 h urinary excretion of calcium was associated with significantly increased U/P and FE of calcium. Also the FE and 24 h excretion of magnesium, a further divalent cation which is transported mainly

Table 1. Plasma data of 8-month-old heterozygous *Umod*^{C93F} mutant mice

	Male Wild-type	Heterozygous	Female Wild-type	Heterozygous
Na^+ (mmol/l)	150.7 ± 3.5	152.4 ± 1.6	147.8 ± 2.4	149.4 ± 1.3
K^+ (mmol/l)	4.71 ± 0.40	5.16 ± 0.26**	4.02 ± 0.24	4.68 ± 0.07***
Ca^{2+} (mmol/l)	2.21 ± 0.06	2.27 ± 0.04*	2.17 ± 0.05	2.27 ± 0.05***
Cl^- (mmol/l)	116.7 ± 2.7	116.4 ± 1.8	113.7 ± 2.5	112.9 ± 1.9
Pi (mmol/l)	1.56 ± 0.19	1.23 ± 0.49	1.30 ± 0.33	0.88 ± 0.19**
Total protein (g/l)	54.4 ± 1.3	54.0 ± 0.9	52.8 ± 1.9	52.0 ± 2.3
Albumin (g/l)	28.7 ± 1.0	28.8 ± 1.0	29.4 ± 1.6	29.8 ± 0.6
Creatinine (μmol/l)	9.1 ± 1.3	10.3 ± 0.9*	10.5 ± 1.4	12.4 ± 1.2**
Urea (mmol/l)	9.6 ± 1.0	21.2 ± 2.1***	10.2 ± 2.3	19.2 ± 2.3***
Cholesterol (mmol/l)	4.88 ± 0.30	4.20 ± 0.28***	3.43 ± 0.34	3.18 ± 0.21
Triglycerides (mmol/l)	4.55 ± 0.99	3.52 ± 0.76*	4.52 ± 0.89	3.22 ± 0.61**
LDH (U/l)	142.8 ± 52.5	123.3 ± 30.7	143.9 ± 25.4	145.5 ± 34.5
ALAT (U/l)	34.2 ± 12.8	27.6 ± 8.8	26.4 ± 2.5	24.6 ± 6.3
ASAT (U/l)	48.0 ± 24.9	42.2 ± 7.0	42.4 ± 3.7	47.0 ± 9.4
AP (U/l)	80.7 ± 5.7	106.0 ± 10.8***	135.0 ± 20.2	169.0 ± 17.5***
Glucose (mmol/l)	8.27 ± 0.70	7.61 ± 0.92	8.24 ± 0.61	7.92 ± 1.51
Lactate (mmol/l)	10.5 ± 1.2	10.0 ± 2.1	9.5 ± 1.1	9.7 ± 1.8
Ferritin (μg/l)	33.6 ± 18.2	20.0 ± 6.2*	40.1 ± 6.5	30.5 ± 8.2**
Transferrin (g/l)	1.59 ± 0.04	1.49 ± 0.05***	1.57 ± 0.05	1.49 ± 0.04**
Iron (μmol/l)	31.5 ± 4.1	28.0 ± 4.2	33.7 ± 3.8	28.7 ± 3.2**

Data are means ± SD. $n = 9–10$ per genotype and gender.
Pi, inorganic phosphorus; LDH, lactate dehydrogenase (EC 1.1.1.27); ALAT, alanine aminotransferase (EC 2.6.1.2); ASAT, aspartate aminotransferase (EC 2.6.1.1); AP, alkaline phosphatase (EC 3.1.3.1).
Umod^{C93F} heterozygous mutant versus wild-type: $^*P < 0.05$; $^{**}P < 0.01$; $^{***}P < 0.001$.

Table 2. Urine data of adult mice under basal conditions and after deprivation of drinking water for 18 h

	Male Wild-type	Heterozygous	Female Wild-type	Heterozygous
Body weight (g)	37.3 ± 4.1	26.6 ± 1.3***	36.3 ± 3.1	23.7 ± 0.9***
Drinking water *ad libitum*				
Water intake (ml/day)	5.08 ± 2.63	5.96 ± 1.30	4.01 ± 1.22	5.85 ± 0.95**
Urine volume (ml/day)	1.33 ± 1.02	2.23 ± 0.84 $^{P = 0.058}$	0.96 ± 0.32	2.04 ± 0.54***
Urine osmolality (mOsm/kg H_2O)	2517 ± 774	1687 ± 457*	2964 ± 661	1727 ± 208***
Na^+ (μmol/day)	176 ± 46	226 ± 76	170 ± 30	238 ± 63*
K^+ (μmol/day)	430 ± 101	620 ± 178*	424 ± 92	598 ± 145*
Ca^{2+} (μmol/day)	2.8 ± 2.3	9.0 ± 4.0**	2.6 ± 0.6	8.1 ± 3.6**
Cl^- (μmol/day)	217 ± 55	282 ± 79 $^{P = 0.061}$	204 ± 44	284 ± 74*
Mg^{2+} (μmol/day)	29.1 ± 9.8	44.0 ± 12.9*	32.5 ± 8.8	51.3 ± 13.7**
Creatinine (μmol/day)	5.8 ± 1.4	6.7 ± 1.9	5.8 ± 0.8	5.4 ± 1.0
Urea (mmol/day)	1.5 ± 0.4	2.0 ± 0.5 $^{P = 0.052}$	1.5 ± 0.3	1.9 ± 0.3*
Uric acid (nmol/day)	932 ± 276	283 ± 91***	1368 ± 160	475 ± 91***
Glucose (μmol/day)	2.1 ± 0.7	2.0 ± 0.7	2.5 ± 0.4	2.0 ± 0.3**
Total protein (mg/day)	10.5 ± 3.0	6.6 ± 2.5**	2.1 ± 0.7	0.8 ± 0.2***
Deprivation of drinking water for 18 h				
Urine volume (ml)	0.64 ± 0.36	0.97 ± 0.34 $^{P = 0.068}$	0.49 ± 0.26	0.73 ± 0.30 $^{P = 0.087}$
Urine osmolality (mOsm/kg H_2O)	3743 ± 631	2498 ± 377***	3898 ± 799	2568 ± 443**

Age of mice analyzed: 9 month. Data are means ± SD. $n = 6–10$ per genotype and gender (details see Supplementary Material, Table S1).
Umod^{C93F} heterozygous mutant versus wild-type: $^*P < 0.05$; $^{**}P < 0.01$; $^{***}P < 0.001$.

paracellularly at the TALH segment like calcium, were significantly increased in heterozygous mutants of both genders compared with wild-type controls. Further, although daily urea excretion was increased in mutants (males: $P = 0.05$, females: $P < 0.05$), U/P and FE of urea were decreased. In contrast to all solutes mentioned above whose daily urinary excretion were increased, 24 h excretion of uric acid was distinctly decreased. Also U/P and FE of uric acid were significantly decreased in heterozygotes. Despite deprivation of drinking water, heterozygotes still excreted more urine than wild-type controls (males: $P = 0.07$, females: $P = 0.09$), whereas urine osmolality remained significantly decreased (Table 2).

Urinary excretion of uromodulin was markedly decreased in *Umod*^{C93F} mutant mice of both genders (Supplementary Material, Fig. S2C). Uromodulin excretion in homozygous mutant mice was more distinctly decreased than in heterozygotes, but they still excreted small amounts of mutant uromodulin. The size of the uromodulin proteins detected in urine of homozygous

Table 3. DXA analysis of weight- and bone-related parameters of adult mice

	Male		Female	
	Wild-type	Heterozygous	Wild-type	Heterozygous
Body weight (g)	38.0 ± 2.0	29.1 ± 1.0***	36.3 ± 6.1	25.2 ± 1.5***
Fat mass (units)	13.7 ± 3.2	4.3 ± 1.2***	16.1 ± 6.8	3.0 ± 1.3***
Fat content (units × 100/g)	35.9 ± 6.6	14.7 ± 3.9***	43.6 ± 15.4	11.8 ± 5.1***
BMD (mg/cm^2)	62.9 ± 1.9	53.3 ± 2.1***	65.7 ± 4.0	53.7 ± 2.8***
BMC (mg)	853 ± 150	540 ± 35***	887 ± 213	491 ± 47***
Bone content (%)	2.24 ± 0.31	1.85 ± 0.09**	2.45 ± 0.48	1.94 ± 0.12**

Age of mice analyzed: 9 month. Data are means ± SD. $n = 10$ per genotype and gender.
BMD, bone mineral density; BMC, bone mineral content.
Umod^{C93F} heterozygous mutant versus wild-type: $^*P < 0.05$; $^{**}P < 0.01$; $^{***}P < 0.001$.

and heterozygous *Umod*^{C93F} mutant mice corresponded to that of the wild-type uromodulin band.

The analysis of the skeleton, performed by DXA analysis, showed that bone-mineral density and bone-mineral content were significantly decreased in 9-month-old heterozygous mutants of both genders, indicating osteopenia (Table 3).

In conclusion, the mouse line *Umod*^{C93F} exhibited similar clinical characteristics as the mouse line *Umod*^{A227T} and UAKD-affected patients.

Characterization of the uromodulin trafficking defect

On light microscopy, kidneys of 4-month-old *Umod*^{C93F} mutants exhibited only discrete histological alterations (Fig. 1), including intracytoplasmic inclusions in TALH cells, visible in Masson-Trichrome-stained paraffin sections (Fig. 1A) and in toluidine blue-stained semi-thin sections (Fig. 1B). Immunohistochemical analysis for uromodulin demonstrated distinct apical membrane staining and weak diffuse homogeneous cytoplasmic staining for uromodulin in TALH cells of wild-type control mice (Fig. 1C left). In contrast, cells of the TALH of mutants exhibited more intense uromodulin staining, which was located intracytoplasmically in the perinuclear compartment (Fig. 1C right), already present at 2 weeks of age (Fig. 1D). Ultrastructural evaluations of TALH cells demonstrated intracytoplasmic perinuclear stacked lamellar structures (Fig. 1E).

To explore if these lamellar structures represent hyperplastic bundles of the ER, double-immunofluorescence analyses of uromodulin with markers for ER (PDI, BiP) and Golgi apparatus (giantin) were performed (Fig. 1F). Strong co-localization of mutant uromodulin with PDI and BiP in TALH cells of *Umod*^{C93F} mutant mice was detected, whereas there was no co-localization with giantin. Similar co-localization of mutant uromodulin to the ER marker but not to the Golgi apparatus marker was also observed in TALH cells of *Umod*^{A227T} mutant mice (data not shown). Due to the structural alterations of TALH cells in *Umod* mutant mice, we performed immunohistochemical analyses for NKCC2, an ion transporter located at the apical membrane of TALH cells, to evaluate if the polarity of TALH cells is affected in mutant mice (Fig. 1G). NKCC2 was localized at the apical membrane of TALH cells in wild-type mice as well as in *Umod* mutant mice of both lines indicating maintenance of TALH cell polarity.

Further, we carried out western blot analyses of kidney extracts from both *Umod* mutant mouse lines (Fig. 1H). Renal uromodulin protein abundance in wild-type mice was detected at a very low level and its molecular weight corresponded to the fully glycosylated mature uromodulin protein excreted with urine. In contrast, abundance of uromodulin protein in kidneys of *Umod* mutant mice was remarkably higher when compared with wild-type mice, and it consisted predominantly of the immature uromodulin protein. Further, uromodulin protein abundance was higher in homozygous *Umod*^{A227T} mutant mice when compared with *Umod*^{A227T} heterozygotes. Signal intensities between *Umod*^{A227T} homozygotes and *Umod*^{C93F} heterozygotes were similar. Moreover, the main fraction of uromodulin detected in kidneys of mutant mice consisted of lower molecular weight immature protein (~100 kDa) than the fully glycosylated uromodulin protein excreted with urine.

Onset of the increase of plasma urea in mutant lines *Umod*^{C93F} and *Umod*^{A227T}

In line *Umod*^{C93F}, 2-week-old heterozygotes exhibited urea levels similar to those of age-matched wild-type littermates (Fig. 2A, Supplementary Material, Fig. S3). At 4 weeks of age, the median of plasma urea concentration tended to be increased in heterozygotes males. At 7 weeks of age, the median of plasma urea levels was significantly increased in female heterozygous mutants and tended to be increased in male heterozygotes. Three-month-old heterozygous *Umod*^{C93F} mutant mice of both genders exhibited significantly increased plasma urea levels compared with wild-type littermate controls. In contrast to heterozygotes, blood urea levels were already significantly increased in male and female homozygotes from 2 weeks of age onwards.

In line *Umod*^{A227T}, 2-week-old homozygotes and heterozygotes exhibited urea levels similar to those of age-matched wild-type littermates (Fig. 2B) (20). At 7 weeks of age, plasma urea levels were moderately but significantly increased in homozygous *Umod*^{A227T} mutants of both genders, resembling the mean urea level of 7-week-old heterozygous *Umod*^{C93F} mutant mice. Four-month-old homozygous and heterozygous *Umod*^{A227T} mutant mice of both genders exhibited significantly increased plasma urea levels compared with wild-type littermate controls.

Comparison of the severity of the decrease of uromodulin excretion between both *Umod* mutant mouse lines

Urinary excretion of uromodulin was markedly decreased in heterozygous *Umod*^{C93F} mutant mice compared with wild-type littermate controls (Fig. 2C). The extent of the decrease in uromodulin excretion in *Umod*^{C93F} heterozygotes was similar to that of *Umod*^{A227T} homozygotes. In both *Umod* mutant mouse lines, uromodulin excretion in homozygous mutant mice was more distinctly decreased than in heterozygotes (Supplementary Material, Fig. S2C) (20).

Impact of the *Umod* mutation on body weight, body composition and postnatal body growth

Nine-month-old heterozygous *Umod*^{C93F} mutants of both genders exhibited a 23–30% lower body weight and a 69–81% reduced fat mass compared with wild-type controls (Table 3). In the mutant mouse line *Umod*^{A227T}, adult mutant mice also exhibited a lower body weight compared with age-matched littermate controls (20). To evaluate the onset of the differences in body weight, we monitored the body weight gain by weighing the animals of the mouse line *Umod*^{C93F} from the day of birth up to 16 weeks of age (Fig. 3). Birth weight did not differ between genotypes. Four-week-old heterozygous mutant males exhibited a significantly reduced body weight compared with wild-type controls, whereas body weight of heterozygotes and wild-types became significantly different from 7 weeks of age onwards in females. Body weights of homozygous mutants of both genders were significantly lower than those of wild-type littermates from 5 weeks of age onwards.

Clinical-chemical and morphological kidney findings in aged *Umod* mutant mice with respect to type of mutation and zygosity

With age, there was a continuous increase of blood urea concentrations in *Umod* mutant mice of both lines (Fig. 4A). Urea excretion and in consequence blood urea concentrations are strongly influenced by the proper tubular function in building up and maintaining of renal corticomedullary urea concentration gradient, similar to the role of salt ions for the corticomedullary osmotic gradient (27). Homozygous mutants had constantly higher blood urea levels than age-matched heterozygous mutant littermates. Further, the increase in blood urea concentration in the *Umod*^{C93F} mouse line was stronger than in age-matched *Umod*^{A227T} mutants of the same allelic status. Further, plasma Cystatin C concentrations, which represent a robust endogenous marker of glomerular filtration rate (28), were significantly increased in homozygous mutants of both lines compared with wild-type littermates at an age of 4 months (Fig. 4B). The Cystatin concentrations did not significantly differ between homozygous *Umod*^{A227T} mutants and homozygous *Umod*^{C93F} mutants. At an age of 20–22 months, *Umod* mutants of both lines had significantly increased Cystatin levels compared with wild-type mice, and homozygous *Umod*^{C93F} mutants exhibited distinctly increased plasma Cystatin C concentrations compared with homozygous *Umod*^{A227T} mutants.

Morphological kidney alterations in aged *Umod* mutant mice comprised interstitial fibrosis and tubular atrophy (IFTA) as well as interstitial infiltrates of inflammatory mononuclear cells, which were mainly localized in the corticomedullary region (Fig. 5A and B). Further, dilatations and cysts of various tubular segments and of Bowman's capsule were inconstant findings in kidneys of aged mutant mice (Fig. 5C). Aged mutants, preferentially of the mouse line *Umod*^{C93F}, exhibited a dilation of the renal pelvis. Immunohistochemical detection of uromodulin in kidneys of aged *Umod* mutant mice revealed, in contrast to young mice, a heterogeneous staining pattern in TALH profiles (Fig. 5D and E). There were TALH profiles where some cells exhibited a strong perinuclear uromodulin immunostaining pattern as seen in TALH cells of young-adult *Umod* mutant mice, whereas other cells of the same TALH profile showed discrete or nearly no uromodulin staining. Ultrastructural analysis of TALH cells of aged *Umod* mutants revealed distinct intracytoplasmic perinuclear stacked lamellar structures as seen in young-adult *Umod* mutant mice, occasionally filling most of the cytoplasmic compartment (Fig. 5F). However, there were also TALH cells with strongly dilated hyperplastic ER in the perinuclear intracytoplasmic compartment, whereas other cells exhibited only discreet or no hyperplastic ER. Hyperplastic ER bundles appeared heterogeneous (Fig. 5G). Thus, in the majority of the TALH cells, hyperplastic ER presented as perinuclear parallel-folded smooth lamellar membranous structures. Other TALH cells contained dilated hyperplastic ER with moderate electron dense material included.

To evaluate putative effects of type of mutation and zygosity on severity of advanced kidney alterations, the two predominant and consistently found kidney alterations IFTA and inflammatory cell infiltrates were quantified with unbiased stereological methods in kidneys of 20- to 22-month-old male mice of the lines *Umod*^{A227T} and *Umod*^{C93F} (Fig. 6). Volume fractions as well as total volumes of IFTA ($Vv_{(IFTA/kid)}$ and $V_{(IFTA,kid)}$, respectively) were significantly higher in homozygous mutants than in heterozygous mutant littermates and were distinctly higher in *Umod*^{C93F} mutants than in *Umod*^{A227T} mutants with the same zygosity. $Vv_{(IFTA/kid)}$ and $V_{(IFTA,kid)}$ of heterozygous *Umod*^{A227T} mutants were similar to wild-type levels. Volume fractions as well as total volumes of inflammatory cell infiltrates ($Vv_{(IC/kid)}$ and $V_{(IC,kid)}$, respectively) were significantly increased in 20- to 22-month-old *Umod*^{C93F} homozygotes and heterozygotes and in *Umod*^{A227T} homozygotes compared with age-matched wild-type mice, but were nearly indifferent when compared between these mutant groups. $Vv_{(IC/kid)}$ and $V_{(IC,kid)}$ of heterozygous *Umod*^{A227T} mutants were similar to wild-type levels.

DISCUSSION

Various clinical phenotypes occur in humans harboring a mutation within the *UMOD* gene and suffering from UAKD. Further, important differences in severity, onset and rate of progression of kidney disease and in age at onset of end-stage renal disease (ESRD) were observed in UAKD affected patients (5). Timepoint of first diagnosis of UAKD and rate of decline of kidney function varies also within affected families harboring the

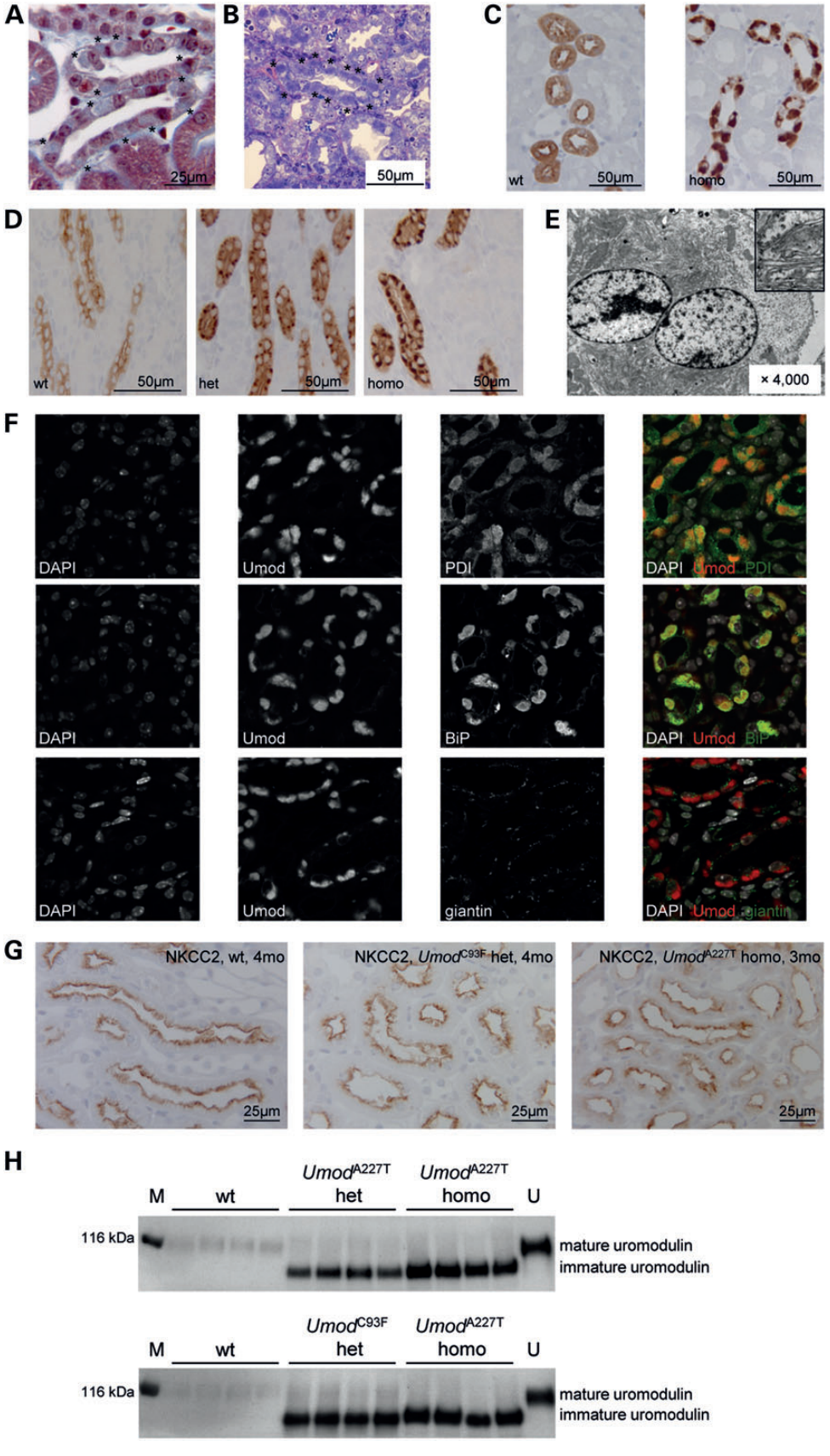

Figure 1. Characterization of the uromodulin trafficking defect. (**A** and **B**) TALH cells of a 4-month-old heterozygous *Umod*^{C93F} mutant mouse contain focal intracytoplasmic inclusions of lamellated trichrome blue material, visible in the Masson-Trichrome (A) and toluidine blue (B) stained kidney section and highlighted by

same mutation. In a study including 37 different UAKD-causing *UMOD* mutations, no relationship between onset and severity of clinical signs as well as renal disease progression and the causative mutation could be demonstrated in humans (5). Important environmental factors or modifier genes were assumed to modulate the clinical UAKD phenotype (5). The two mouse lines *Umod*^{C93F} and *Umod*^{A227T} harbor a mutation within the *Umod* gene and exhibit a progressive renal phenotype with an impairment in the urinary concentrating ability, strongly reduced fractional excretion of uric acid, altered divalent mineral cation metabolism and progressive morphological kidney alterations, which are features highly similar to the characteristics of human UAKD. Both *Umod* mutant mouse lines, which are housed under the same environmental conditions, originate from the same C3H inbred strain and differ only in the *Umod* mutation, therefore making them unique animal models for determining the mutation-specific impact on onset, severity and progression of renal dysfunction in UAKD.

The point mutation of the line *Umod*^{C93F} leads to the amino acid exchange C93F resulting in the loss of the putative disulfide bond C93–C105 (www.uniprot.org/uniprot/Q91X17). In UAKD-affected humans, many known *UMOD* mutations affect the amino acid cysteine. From the more than 70 known *UMOD* mutations at more than 50 amino acid positions, 23 different cysteines are affected, thereof one is C106Y corresponding to murine C105 (3–5). Formation of intrachain disulfide bonds might be essential to exhibit the accurate tertiary structure of uromodulin. Thus, many *UMOD* mutations resulting in a UAKD disease phenotype cause disruption of the molecule's stable tertiary structure, resulting in altered protein folding, retention within the endoplasmic reticulum (ER) and impaired trafficking (6). Similar to the immunohistochemical renal data of affected humans and of *Umod*^{A227T} mutant mice (2,6,8,20), massive intracellular accumulation of immature uromodulin was detected in TALH cells of *Umod*^{C93F} mutant mice. Thus, the immature, not fully glycosylated uromodulin was retained in the ER of TALH cells of mutant mice. Further, intratubular heterogeneity of uromodulin immunostaining in TALH cells, found in aged *Umod* mutant mice, was described also in UAKD-affected humans (29). In consequence, the ER became hyperplastic and the protein abundance of molecular chaperones like PDI or BiP (29) was strongly increased in TALH cells, indicating the initiation of unfolded protein response (UPR) (30,31). In consequence, protein misfolding of mutant uromodulin might compromise ER homeostasis and volume expansion of the ER. Thus, the activation of transcription of molecular chaperones like BiP has been described as a cellular mechanism to increase protein-folding capacity and to reduce ER stress (30,32). Further studies are necessary to get more insights into the mechanisms of UAKD associated ER stress. The Golgi apparatus of TALH cells appeared to be unaffected, as no co-localization of uromodulin with giantin was detected. Maturation retardation of mutant uromodulin also impeded protein folding and processing of native uromodulin protein to the apical membrane of TALH cells and its release and excretion in the urine. Thus, uromodulin excretion in heterozygous *Umod*^{C93F} mutant mice was decreased to $<50\%$ of wild-type levels caused by the dominant negative effect of mutant protein on the maturation of native uromodulin. In UAKD patients, a strong decrease of uromodulin excretion was a nearly constant finding in heterozygous *UMOD* mutation carriers (6,9,33,34). In consequence of the severe structural alterations of TALH cells due to ER hyperplasia and disturbance of ER homeostasis, TALH dysfunction occurs. The mechanism of TALH dysfunction was already proposed in the description of the mutant mouse line *Umod*^{A227T} (20) and is now supported by the results of kidney function analyses of *Umod*^{C93F} mutant mice. However, at least the polarity of TALH cells seemed to be intact in both *Umod* mutant mouse strains, as the ion transporter NKCC2 remained strictly located at the apical membrane of TALH cells. UAKD in humans is described as progressive renal disease which inconstantly can lead to end-stage kidney disease (8,35). Advanced histological alterations, which can be observed in kidneys of humans suffering from UAKD, are tubulointerstitial fibrosis, interstitial infiltrates of inflammatory mononuclear cells, tubular atrophy and, in approximately one-third of patients, uni- or bilateral tubular or glomerular cysts (5,6,8,36–40), alterations which we also observed in kidneys of aged *Umod* mutant mice of both mouse lines. Long-lasting ER stress of TALH cells might induce a profibrotic and proinflammatory microenvironment leading to peritubular fibrosis and mononuclear infiltrates, beginning in the corticomedullary TALH region. Of note, impaired ER function of renal tubular cells might increase vulnerability to ER stress and, if ER dysfunction is long-lasting, it leads to peritubular fibrosis and tubular atrophy (41). Tubulo-interstitial fibrosis represents the hallmark of progression of chronic kidney disease, and epithelial damage can initiate a pro-fibrotic microenvironment (42). Increase of the severity of the uromodulin maturation

stars. (**C**) Representative TALH profile immunohistochemically stained for uromodulin of a 4-month-old wild-type (left) and heterozygous *Umod*^{C93F} mutant (right) mouse. In wild-type mice, weak diffuse homogeneous cytoplasmic and distinct apical membrane staining for uromodulin in TALH cells was observed. TALH cells of mutants exhibited a strong perinuclear staining intensity in the cytoplasm. (**D**) Representative TALH profile immunohistochemically stained for uromodulin of 2-week-old wild-type (left), heterozygous (middle) and homozygous (right) *Umod*^{C93F} mutant mice. Intracytoplasmic accumulation of uromodulin was already present in mutants at an age of 2 weeks. (**E**) Representative electron micrograph of TALH cells of a 4-month-old heterozygous *Umod*^{C93F} mutant mouse; final magnification $\times 4000$, final magnification of insert $\times 20\,000$. TALH cells contained intracytoplasmic inclusions composed of perinuclear stacked lamellar structures (magnification in insert). (**F**) ER retention of uromodulin in TALH cells of a heterozygous *Umod*^{C93F} mutant mouse, demonstrated by confocal laser scanning microscopy. Uromodulin is co-localized with the molecular chaperones PDI (upper row) and BiP (middle row), localized in the ER, but not with giantin (lower row), which is localized in the Golgi apparatus. Of further interest is the strong expression of PDI and BiP in TALH cells, indicating hyperplasia of ER. (**G**) Representative TALH profiles immunohistochemically stained for NKCC2 of a 4-month-old wild-type, a 4-month-old heterozygous *Umod*^{C93F} mutant and a 3-month-old homozygous *Umod*^{A227T} mutant mouse. The ion transporter NKCC2 is localized at the apical membrane of TALH cells in wild-type mice as well as in *Umod* mutant mice of both lines demonstrating that accurate polarity of TALH cells is present in *Umod* mutant mice. (**H**) Analysis of uromodulin protein abundance in whole kidney homogenates of 3-month-old wild-type and *Umod* mutant mice. In kidneys of wild-type mice, uromodulin is abundant at a very low level, and its molecular size corresponded to the fully glycosylated uromodulin protein excreted with urine. In contrast, molecular weight of the main fraction of uromodulin detected in mutant mice was lower than the fully glycosylated uromodulin protein excreted with urine, indicating the accumulation of immature uromodulin in kidneys of *Umod* mutant mice. Uromodulin abundance in kidneys of *Umod* mutant mice was remarkably higher when compared with wild-type mice. M, protein molecular weight marker; wt, wild-type mouse, het, heterozygous mutant mouse, homo, homozygous mutant mouse; U, urine.

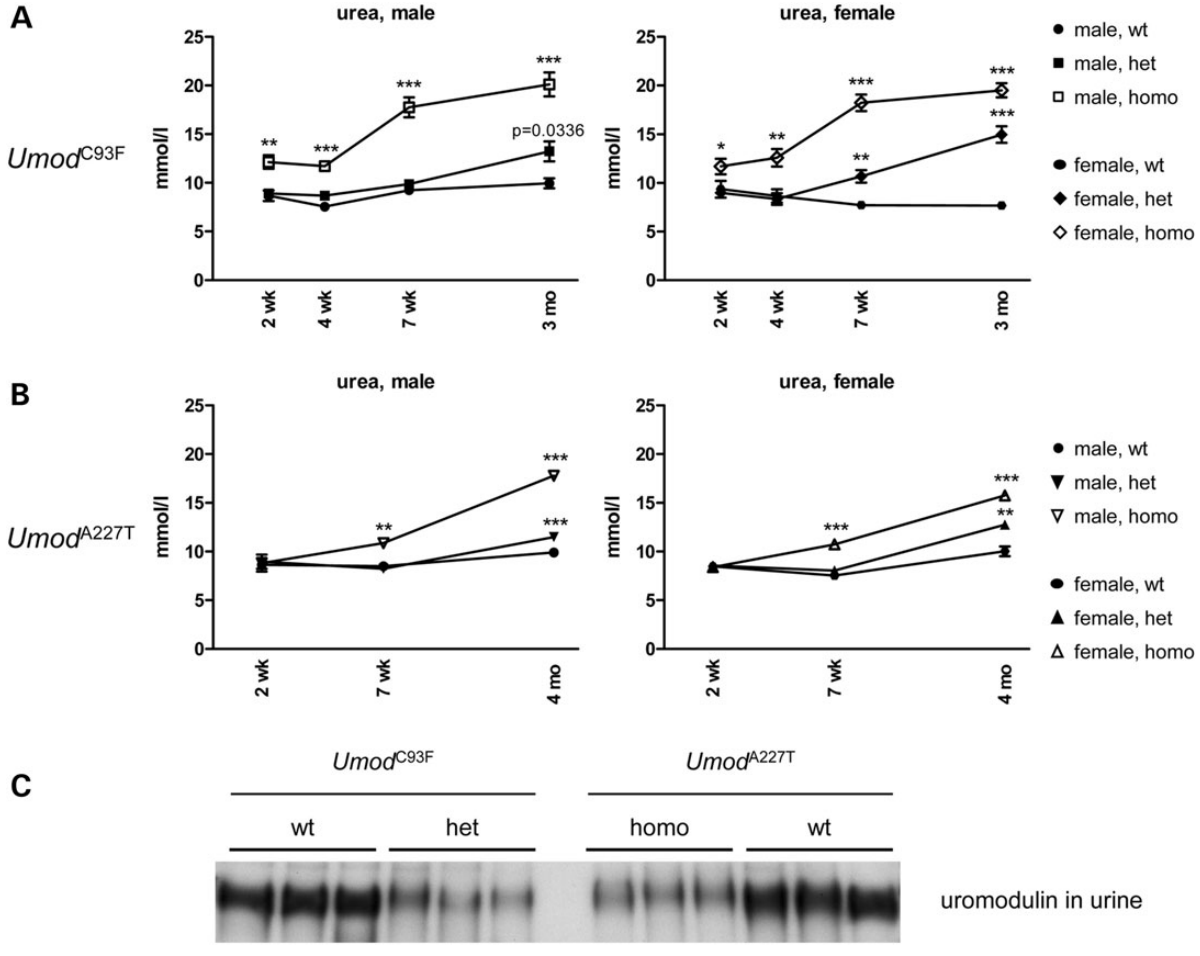

Figure 2. Onset and severity of the clinical phenotype of *Umod*^{C93F} and *Umod*^{A227T} mutant mice. (**A**) Analysis of the onset of the increase of plasma urea of *Umod*^{C93F} mutant mice. Data points show means ± SEM. $n = 5–22$ per genotype and gender (details see Supplementary Material, Table S1). (**B**) Analysis of the onset of the increase of plasma urea of *Umod*^{A227T} mutant mice. Data points show means ± SEM. $n = 4–18$ per genotype and gender (details see Supplementary Material, Table S1). (A and B) *Umod* mutants versus wild-type: $^{*}P < 0.05$; $^{**}P < 0.01$; $^{***}P < 0.001$. (**C**) Urine analysis of uromodulin excretion demonstrates that uromodulin excretion of *Umod*^{C93F} heterozygotes and *Umod*^{A227T} homozygous mutants is decreased at a similar range compared with wild-type controls. (A–C) Wt, wild-type; het, heterozygous mutant; homo, homozygous mutant. The corresponding mutant mouse line is indicated.

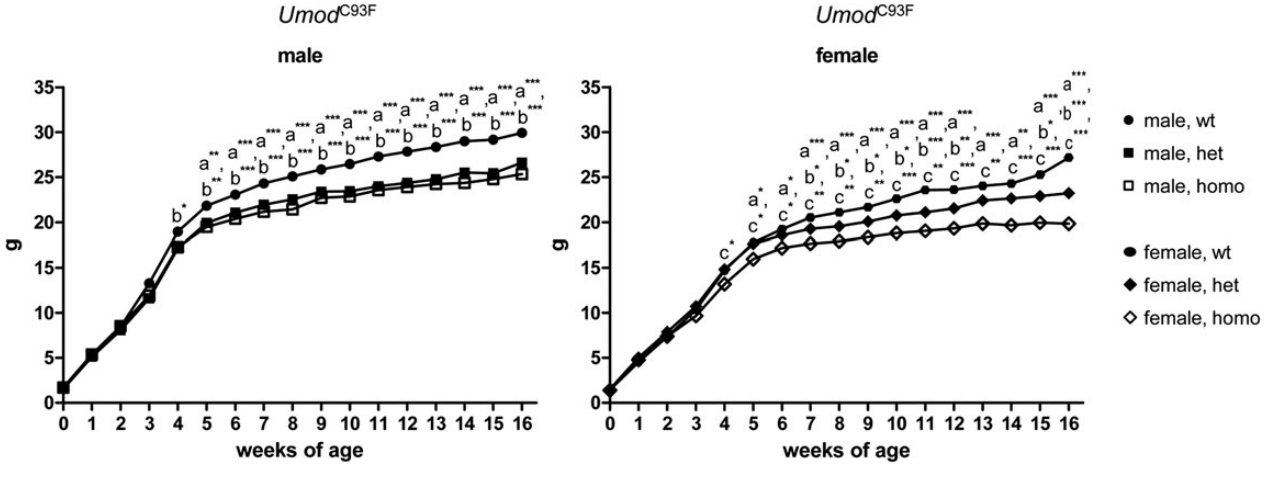

Figure 3. Postnatal body growth of *Umod*^{C93F} mutant mice. Growth curves of *Umod*^{C93F} mutant mice shows that significantly decreased body weights of mutant mice were present already at an age of 4 weeks in males and of 5 weeks in females. Data points show means. Age 0–10 weeks: $n = 11–48$ per genotype and gender; age 11–16 weeks: $n = 5–29$ per genotype and gender (details see Supplementary Material, Table S1). $^{*}P < 0.05$; $^{**}P < 0.01$; $^{***}P < 0.001$; ^{a}homozygous versus wild-type; ^{b}heterozygous versus wild-type; ^{c}homozygous versus heterozygous. Wt, wild-type; het, heterozygous mutant; homo, homozygous mutant.

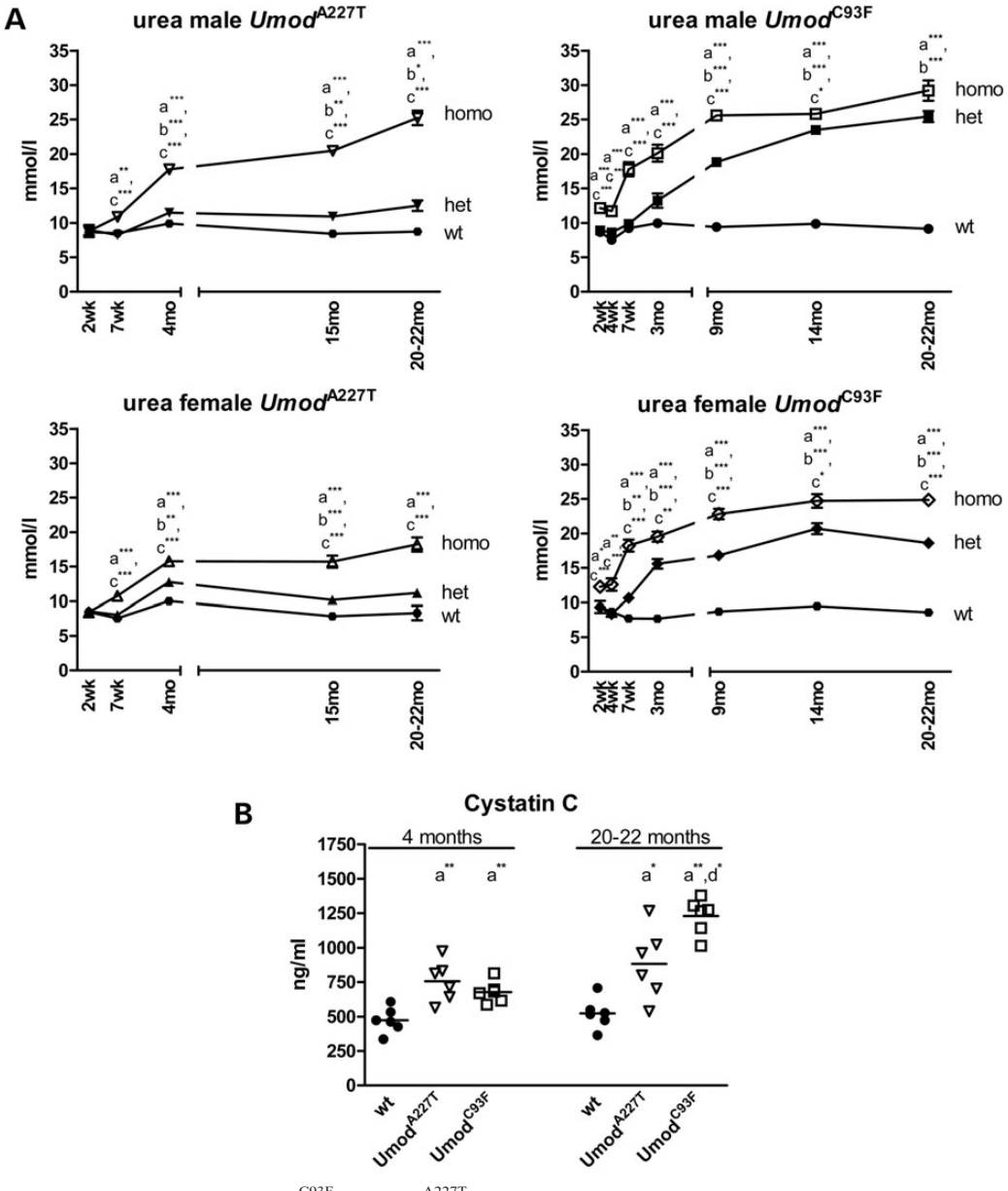

Figure 4. Progression of the clinical phenotype of *Umod*^{C93F} and *Umod*^{A227T} mutant mice with age. (**A**) Progression of the clinical phenotype was demonstrated by continuous increase of plasma urea of *Umod*^{A227T} and *Umod*^{C93F} mutant mice with age. Data points show means ± SEM. $n = 3–22$ per genotype and age group (details see Supplementary Material, Table S1). (**B**) Plasma Cystatin C concentration in male homozygous *Umod*^{A227T} and *Umod*^{C93F} mutant and wild-type mice at an age of 4 months and 20–22 months. Data show scatter dot plot and means. $n = 6$ per genotype and age group. $^{*}P < 0.05$; $^{**}P < 0.01$; $^{***}P < 0.001$; [a]homozygous versus wild-type; [b]heterozygous versus wild-type; [c]homozygous versus heterozygous of the same *Umod* mutant line; [d]homozygous *Umod*^{C93F} mutant versus homozygous *Umod*^{A227T} mutant. Wt, wild-type; het, heterozygous mutant; homo, homozygous mutant.

retardation and in consequence the ER stress of TALH cells might result in higher occurrence of peritubular interstitial fibrosis. Renal dysfunction progresses with age in *Umod* mutant mice, and progressed structural alterations like IFTA might contribute to disease progression. Bohle *et al*. (43) postulated already more than two decades ago that there might be a close correlation between the degree of interstitial fibrosis and the loss of renal urine concentrating ability in chronic kidney disease, regardless of the primary pathological event (42).

The presumed sequence of events in the pathophysiology and progression of UAKD is schematically summarized in Figure 7. Thus, the initial event is a mutation of the uromodulin gene leading to the disruption of the molecule's physiological tertiary structure. In consequence, the maturation of the mutant protein is retarded; also affecting the processing of the native uromodulin protein and leading to ER hyperplasia and UPR as well as to decreased uromodulin excretion. To a certain degree, the uromodulin trafficking defect might be compensated by TALH cells until TALH dysfunction appears. TALH dysfunction can be compensated to a certain degree from the other segments of the nephron until clinical signs occur. Thus, 2-week-old *Umod*^{C93F} heterozygotes already exhibit retention of uromodulin in TALH cells but no increase in plasma urea. This development might occur as a cumulative process. After transgression of

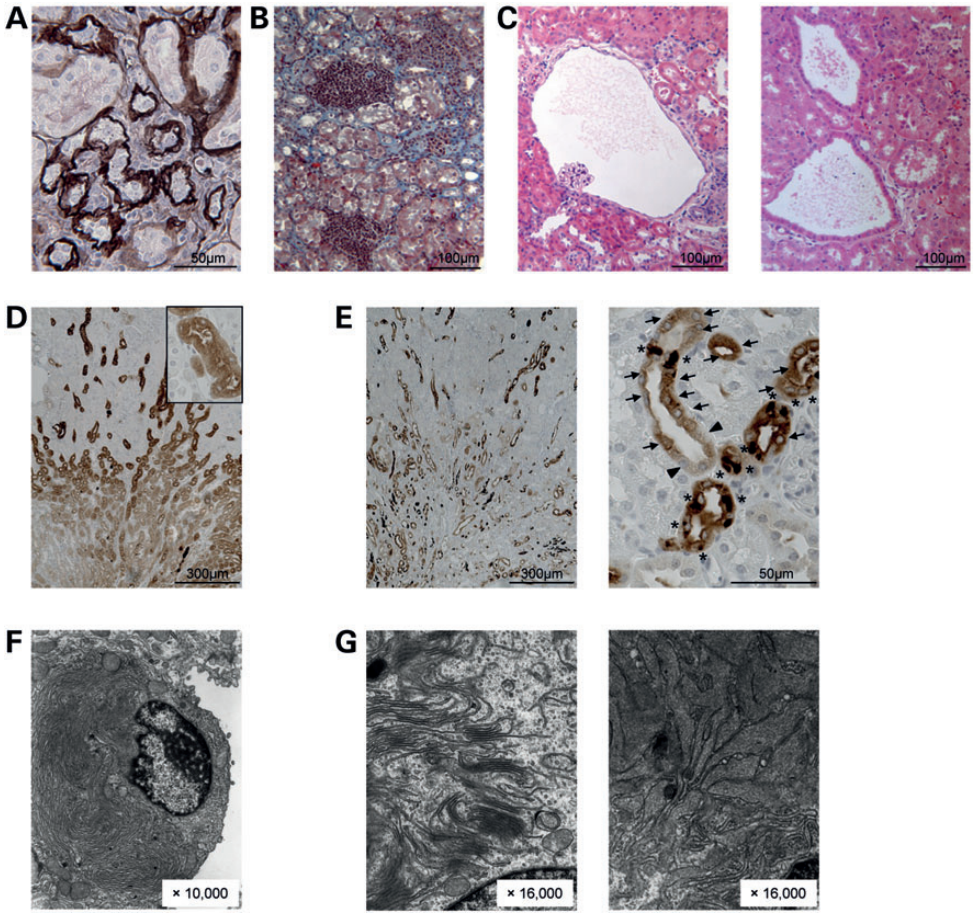

Figure 5. Morphological kidney alterations of aged *Umod* mutant mice. (**A** and **B**) Consistently found morphological alterations in kidneys of *Umod* mutants were (A) interstitial fibrosis and tubular atrophy (IFTA) and (B) interstitial infiltrates of inflammatory mononuclear cells, consisting predominantly of lymphocytes, located predominantly in the corticomedullary region. (**C**) Cystic changes of Bowman's capsule (left site) and tubules (right site). A: PAS-silver; B: Masson-Trichrom; C: H&E. A–C: 20-month-old heterozygous $Umod^{C93F}$ mutant mice. (**D** and **E**) Representative kidney TALH profiles immunohistochemically stained for uromodulin of a 20-month-old wild-type (D), as well as of a 20-month-old heterozygous $Umod^{C93F}$ mutant mouse (**E**). In the 20-month-old wild-type mouse, TALH segments are arranged radially within the kidney, and staining of uromodulin in TALH cells were enforced in the apical membrane and weak, diffuse and homogenous in the cytoplasm (D). In contrast, TALH segments in the *Umod* mutant mouse kidneys appear disarranged (E, left side). Heterogeneity of uromodulin staining pattern is present even within TALH profiles. TALH cells with distinct perinuclear uromodulin staining (asterisk) are present, whereas other TALH cells exhibit weak diffuse cytoplasmic staining pattern (arrow) or (nearly) no uromodulin staining (arrow head). Twenty-month-old heterozygous $Umod^{C93F}$ mutant mouse (E). (**F** and **G**) Ultrastructural aspects of TALH cells of aged *Umod* mutant mice: some TALH cells exhibiting cytoplasm fully filled with stacked lamellar structures representing hyperplastic ER (F). Heterogeneity of hyperplastic ER varied from perinuclear parallel-folded smooth lamellar membranous structures (G, left) to dilated hyperplastic ER including diffuse moderate electron dense material (G, right). Twenty-one-month-old heterozygous $Umod^{C93F}$ mutant mice, final magnifications are indicated (F and G).

an unknown threshold, kidney dysfunction becomes clinically apparent. The cut-off level of the development of clinical signs is highly dependent on the severity of the maturation defect of uromodulin caused by the *UMOD* mutation. Thus, the amino acid-exchange C93F caused a more severe uromodulin maturation defect than A227T in mice, resulting in an earlier onset and increased severity of clinical findings in mutant mice. Hallmarks of early clinical appearance are reduced fractional excretion of uric acid [leading to commonly observed hyperuricemia in humans due to absent uricase activity which is preserved in mice (44)], azotemia, mild defect in urinary concentration ability and decreased uromodulin excretion. Long-term effect of ER stress on TALH cells leads to chronic morphological kidney alterations like interstitial fibrosis, tubular atrophy and interstitial infiltrates of inflammatory cells. Occasionally, tubular and glomerular cyst formation occurs, whose pathophysiology is yet unknown.

Clinical phenotype, onset, severity and progression of UAKD in humans are very heterogeneous, and no association between the type of *UMOD* mutation and clinical appearance could be proved so far. There were several attempts to classify *UMOD* mutations (5,9,11). Thus, e.g. according to their results of *in vitro* assays, Williams *et al*. (11) suggested to classify *UMOD* mutations according to the severity of the protein maturation defect: group A mutations showing reduced *in vitro* maturation of uromodulin of about 50% when compared with wild-type, and group B mutations showing maturation of about 25% of precursor uromodulin. However, these authors found no correlation of genotype and phenotype *in vivo* as no phenotypic differences of clinical features in patients with group A mutations compared with those with group B mutations were identified. Besides the problems to confer *in vitro* results to the *in vivo* situation, additional variables are discussed like genetic heterogeneity (e.g. modifier genes) and/or different environmental conditions

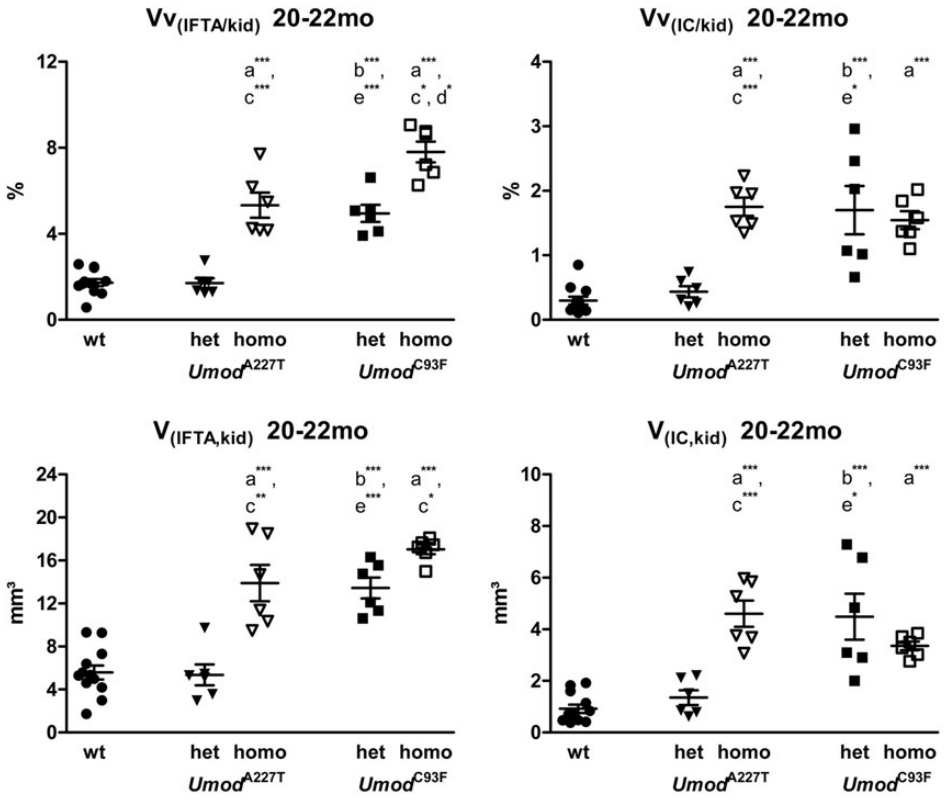

Figure 6. Quantitative evaluation of morphological kidney alterations of aged *Umod* mutant mice. Volume fraction (Vv) and total volume (V) of IFTA ($Vv_{(IFTA/kid)}$ and $V_{(IFTA,kid)}$) and inflammatory cell infiltrates ($Vv_{(IC/kid)}$ and $V_{(IC,kid)}$) of 20–22-month-old male mice of the lines *Umod*^{A227T} and *Umod*^{C93F}. Data points show means ± SEM. $n = 12$ of wild-types, $n = 6$ per genotype and line of mutants. $^{*}P < 0.05$; $^{**}P < 0.01$; $^{***}P < 0.001$; [a]homozygous versus wild-type; [b]heterozygous versus wild-type; [c]homozygous versus heterozygous of the same *Umod* mutant line; [d]homozygous *Umod*^{C93F} mutant versus homozygous *Umod*^{A227T} mutant; [e]heterozygous *Umod*^{C93F} mutant versus heterozygous *Umod*^{A227T} mutant.

(e.g. nutrition) potentially influencing onset, severity and progression of this kidney disease in humans (5) (Fig. 7, Table 4). These parameters were highly standardized in the analyses of our both *Umod* mutant mouse lines, as they differ genetically only in their type of *Umod* mutation and were housed under identical environmental and nutritional conditions. The phenotype of the lines *Umod*^{C93F} and *Umod*^{A227T} is highly similar, but they differ in onset, severity and speed of progression of renal alterations (Table 4). Maturation retardation of mutant C93F uromodulin is much more severe than of mutant A227T uromodulin protein. In consequence, TALH dysfunction becomes clinically apparent at an earlier age and is more severe in *Umod*^{C93F} mutants than in *Umod*^{A227T} mutant mice. *In vitro* analyses demonstrated that also *UMOD* mutations identified in humans differ in their potential to delay uromodulin maturation and trafficking (9,11). The trafficking defect caused by mutant uromodulin might also affect the trafficking of wild-type uromodulin protein in heterozygotes as the uromodulin excretion of *Umod*^{C93F} heterozygous mutant mice is reduced to $<50\%$ of that of wild-type mice. In humans, heterozygous carriers of *UMOD* mutations suffering from UAKD exhibit a decrease of urinary uromodulin of 30% up to $<2\%$ compared with values of control groups (9,33). The potential dominant negative role of mutant uromodulin on the maturation and trafficking of wild-type protein might depend on the severity of disturbance of ER homeostasis (32). Homozygous mutant mice of both *Umod* mutant lines exhibit an earlier onset and more pronounced renal dysfunction than their heterozygous mutant littermates. This is in line with a human report about a consanguineous family, where homozygous carriers of a *UMOD* mutation had a more pronounced renal dysfunction on average than heterozygous carriers (45), indicating the importance of allelic status on onset and speed of progression of the disease.

Besides the alterations of kidney function, both *Umod* mutations affect body growth and body composition. Already at adolescence, *Umod*^{C93F} mutant mice exhibited a reduced body weight compared with wild-type controls. This occurs at the time period where also renal function of the animals starts to be impaired. Thus, reduced body weight gain of mutant mice is not a consequence of azotemia and chronic renal insufficiency, as young mutant mice exhibit only mild signs of renal dysfunction. Other groups published two transgenic mouse lines, the first expressing C148W human mutant uromodulin but exhibiting no clinical renal phenotype even in aged mice and the later expressing the corresponding C147W murine mutant uromodulin exhibiting a clinical phenotype with features of UAKD and renal failure with tubular necrosis at an age of 6 months (46,47). None of both transgenic mouse lines exhibited alterations in body weight. The phenotypic differences between the mutant mouse lines *Umod*^{A227T} and *Umod*^{C93F} and the two transgenic mouse models might be due to a different expression level of uromodulin (endogenous versus transgene expression) and to the different genetic background (C3HeB/FeJ versus C57BL/6 and FVB/N, respectively). Besides alterations in body weight

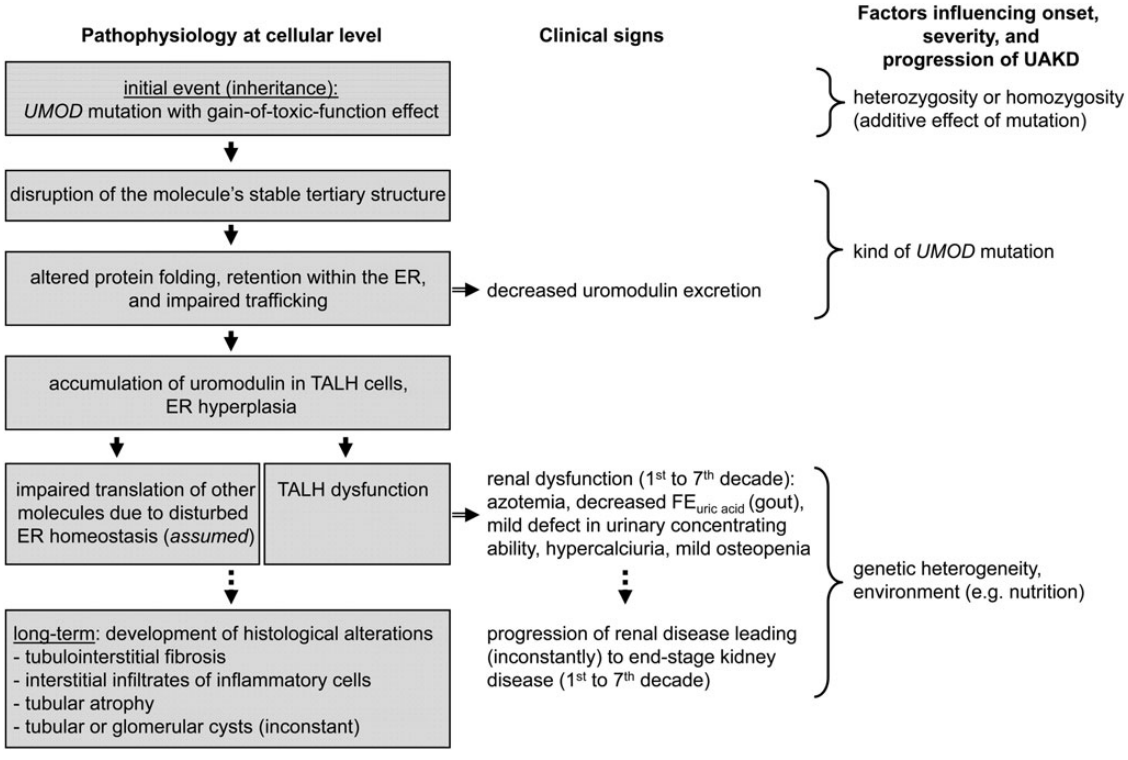

Figure 7. Proposed model of the pathogenesis in UAKD. Pathogenesis of UAKD includes alterations occurring at the cellular level, the resulting clinical findings and parameters which influence onset, severity and progression of clinical signs. First diagnosis of renal dysfunction and/or hyperuricemia in humans suffering from UAKD is reported from 9 months up to 65 years of age (5,6,9,35,39,45,54). End-stage renal disease (ESRD) was diagnosed on some but not all humans suffering from UAKD, whereas the patients with ESRD had an age of 6 up to 66 years of age (most of them >40 years) (9,35,38,45,55). Progressed histopathological alterations described in the kidneys of humans suffering from UAKD are interstitial fibrosis, thickened basement membrane, interstitial infiltrates of inflammatory mononuclear cells, tubular atrophy and, rarely, tubular or glomerular cysts (8,35,36,38,40).

and body composition, phenotypic analysis of both *Umod*^{A227T} and *Umod*^{C93F} mutant mice revealed alterations in plasma concentrations of cholesterol and triglycerides versus wild-type littermates. These findings could be mouse strain-specific and require further investigations.

Taken together, the new established mutant mouse line *Umod*^{C93F} represents a further mutant animal model for UAKD, with the disruption of a putative disulfide bond which is also absent in a known human *UMOD* mutation. Both mutant lines, *Umod*^{C93F} and *Umod*^{A227T}, exhibit phenotypes highly similar to UAKD in humans. Common features of UAKD are TALH dysfunction due to a gain-of-toxic function mutation of *Umod*, causing reduced fractional excretion of uric acid, impaired urinary concentration ability and uremia. Onset, severity and progression of renal dysfunction strongly depend on the particular *Umod* mutation and the zygosity status, which in turn can be attributed to the severity of the processing and trafficking defect of uromodulin. Further studies have to address the UPR pathway as a potential target for new therapeutic strategies and to elucidate the signaling pathways responsible for the initiation of tubular fibrosis in UAKD.

MATERIALS AND METHODS

Animals, linkage analysis and detection of the causative mutation

The mutant mouse lines UREHD1 (25) and the recently characterized mouse line *Umod*^{A227T} (20) were used in this study. Both mouse lines were established within the Munich ENU mouse mutagenesis project which was carried out on the inbred C3HeB/FeJ (C3H) genetic background (25,48). Mouse husbandry and breeding were described previously (25). All animal experiments were carried out under the approval of the responsible animal welfare authority.

Line UREHD1 exhibited an increase of plasma urea which was heritable in an autosomal-dominant manner. For linkage analyses, phenotypic UREHD1 mutant mice were mated to BALB/c mice for two generations, and G1 and G2 offspring were phenotypically classified in mice exhibiting normal or increased plasma urea levels, respectively. DNA of phenotypic mutant G2 offspring were used for genome-wide linkage analyses and further fine mapping as described previously (20,25). *Umod* (NM_009470) was selected for sequence analysis as a positional candidate gene. Genotyping of mice was performed by allele-specific PCR. Primer sequences are available on request.

Clinical-chemical analyses

Analyses of blood and urine parameters were carried out as described previously (20,49). Plasma creatinine values were determined enzymatically (Biomed), while urine creatinine concentration was determined by the Jaffé method. Cystatin C concentration in plasma was determined by the mouse Cystatin C ELISA (BioVendor) as used elsewhere (50).

Table 4. Features of alterations in UAKD and comparison between line *Umod*^{C93F}, line *Umod*^{A227T} and UAKD in humans

(I) Features of alterations in UAKD					
Parameter	Mutant mice				Human
Histological alterations					
Of TALH cells	Accumulation of uromodulin				Accumulation of uromodulin
	ER hyperplasia				ER hyperplasia
Of the kidney	Interstitial fibrosis (aged mice)				Interstitial fibrosis (progressed alterations)
	Interstitial infiltrates (aged mice)				Interstitial infiltrates (progressed alterations)
	Tubular or glomerular cysts (aged mice)				Tubular or glomerular cysts (inconstant)
	Tubular atrophy (aged mice)				Tubular atrophy
Clinical findings					
Renal findings	Azotemia				Azotemia
	Reduced $FE_{uric\ acid}$				Reduced $FE_{uric\ acid}$
	Urinary concentration defect				Urinary concentration defect
	Reduced excretion of uromodulin				Reduced excretion of uromodulin
Extrarenal findings	Alteration in energy metabolism				No data available
	Mild osteopenia				
(II) Comparison between line *Umod*^{C93F}, line *Umod*^{A227T} and UAKD in humans					
(A) Cellular level					
Parameter	*Umod*^{A227T}		*Umod*^{C93F}		UAKD in humans
	het	Homo	het	homo	
Onset of maturation defect	n.d.	n.d.	Already present at 2 weeks of age		No data available
Severity of maturation defect (*parameter:* uromodulin excretion)	+	++	++	+++	*In-vitro*: mutations classified in two groups of severity, however, no correlation to *in-vivo* data
(B) Clinical findings					
Parameter	*Umod*^{A227T}		*Umod*^{C93F}		UAKD in humans
	het	homo	het	homo	
Onset of hyperuricemia/gout	—	—	—	—	First diagnosis: 1st to 7th decade, no correlation to the mutation
Onset of increase of plasma urea	4 months	7 weeks	3 months (m)	2 weeks (m)	
			7 weeks (f)	2 weeks (f)	
Severity of kidney dysfunction	+	++	++	+++	No correlation to the mutation
(C) Parameters influencing onset, severity and progression of UAKD					
Parameter	Mutant mice				Human
Zygosity	Homozygote >> Heterozygote				Homozygote >> Heterozygote (assumed, one case report)
Type of *Umod* mutation	C93F >> A227T				Assumed by *in-vitro* data, however, no correlation to *in-vivo* data
Genetic background	Same inbred mouse strain (C3H)				Heterogeneous (putative impact of modifier genes)
Environment (e.g. housing, nutrition)	Identical				Heterogeneous

$FE_{uric\ acid}$, fractional excretion of uric acid; n.d., not done; +, ++, +++: degree of alterations of the corresponding parameter; m, male; f, female.

Analyses of urine and kidney function

Body weight, water consumption and urine excretion were measured using metabolic cages for single mice (Tecniplast). Urine osmolality was determined by freezing point depression analysis. Daily excretion of solutes was measured. Performance of metabolic cage analyses, calculations of creatinine clearance and of fractional excretion of a solute x (FEx) was performed as described previously (20,51).

Body growth and skeletal analysis

To determine postnatal body growth, measurement of body weight started at day of birth (d0) or one day after (d1), and was performed weekly until an age of 18 weeks. Body weights of mice were determined to the nearest 0.1 g. For skeletal analysis, dual-energy X-ray absorptiometry (DXA) analyses were performed as described (20,49).

Morphological analysis

Histological analyses of kidneys were performed as described previously (20). Staining of histological kidney sections included hematoxylin and eosin (H&E), Giemsa, Masson-Trichrom and PAS-silver for paraffin sections and toluidine blue for semi-thin sections. Immunohistochemistry using the indirect immunoperoxidase technique was performed with a rabbit polyclonal antibody against human THP (H-135; Santa Cruz Biotechnology) and a rabbit polyclonal antibody against rat NKCC2 (Alpha Diagnostic International). For electronmicroscopic analysis, kidneys were fixed with 3% glutaraldehyde in PBS (pH 7.2) via orthograde vascular perfusion, 1 mm^3 samples of the renal cortex were postfixed by immersion with the same fixative for one day and processed as described (25).

Colocalization of uromodulin with the two ER markers protein disulphide isomerase (PDI) and 78 kDa glucose regulated protein (GRP78, BiP), and the Golgi maker giantin was studied by multicolor immunofluorescence. The following primary antibodies were used: polyclonal goat antiserum against human uromucoid (MP Biomedicals), polyclonal rabbit anti PDI IgG (Abcam), polyclonal rabbit anti GRP78/BiP IgG (Abcam) and polyclonal rabbit anti giantin IgG (Abcam). All secondary antibodies were produced in donkey and coupled to FITC or Cy3 (Dianova). Embedding of slides was done with Vectashield antifade solution (Vector

Laboratories) containing DAPI as a nuclear counterstain. Confocal optical sections (pixel size 50 × 50 nm, pinhole size 1 Airy unit corresponding to an optical thickness of 0.7–1 μm) were recorded using a confocal laser scanning microscope (LSM 510 Meta; Zeiss) equipped with a 40× Plan-Neofluar oil immersion objective (NA 1.3). A polychromatic multichannel detector (Meta detector; Zeiss) was used to discriminate autofluorescence from immunofluorescence signals.

Volume fractions of IFTA and inflammatory cell infiltrates in the kidney ($Vv_{(IFTA/kid)}$ and $Vv_{(IC/kid)}$) were determined by the point-counting method (52) using systematically sampled paraffin kidney sections (PAS-silver stained sections for IFTA and Giemsa stained sections for IC). Test fields were selected in paraffin sections by systematic random sampling using an image analyzing system which consisted of a light microscope (BX41, Olympus, Germany), a color video camera (DP72, Olympus, Germany) and the software new CASTTM (computer-assisted stereological toolbox, Visiopharm, Denmark). $Vv_{(IFTA/kid)}$ and $Vv_{(IC/kid)}$ were calculated by dividing the sum of points hitting IFTA and inflammatory cell infiltrates, respectively [$\sum$P(IFTA) and $\sum P_{(IC)}$] by the sum of points hitting renal tissue [$\sum$P(kid)]. The kidney volume ($V_{(kid)}$) was calculated by dividing its weight by its specific weight (1.05 mg/mm^3). The total volumes of IFTA and inflammatory cells ($V_{(IFTA,kid)}$ and $V_{(IC,kid)}$) were calculated as the products of the respective volume fraction ($Vv_{(IFTA/kid)}$ and $Vv_{(IC\ /kid)}$) and $V_{(kid)}$.

Western blot analyses

Twenty-four-hour urine samples, standardized for equal creatinine levels, were denatured by boiling after addition of beta-mercaptoethanol and loaded on 8% SDS-polyacrylamide minigels. Blotting and immunodetection were performed as described (53). For detection of urinary uromodulin, goat antiserum against human uromucoid (MP Biomedicals) was used. Signal intensities were quantified using ImageQuant (GE Healthcare).

For western blot analyses of renal homogenates, whole kidneys were homogenized in extraction buffer (20 mM Tris, 2% Triton-X100, 20% 5× Laemmli buffer). Protein concentration was determined by BCA assay. Equal amounts of denatured proteins were loaded per lane on 8% SDS-polyacrylamide minigels. For detection of renal uromodulin, a rabbit polyclonal antibody against human THP (H-135; Santa Cruz Biotechnology) was used.

Statistical analysis

Data are shown as means ± SD or SEM as indicated. If the sum of n_1 and $n_2 \leq 15$, data were analyzed by using exact Fisher–Pitman test. If the number of animals tested and compared were >15 (sum of n_1 and n_2), unpaired Student's *t*-tests were used. In cases of multiple comparisons, Holm-Bonferroni correction was performed. Detailed information about the number of animals per experiment is given in Supplementary Material, Table S1.

SUPPLEMENTARY MATERIAL

Supplementary Material is available at *HMG* online.

ACKNOWLEDGEMENTS

We thank Dr Sven Reese, bioinformatician of the veterinary faculty of Munich, for his support in statistical analysis, Angela Siebert for excellent technical assistance on electron microscopic analyses, the company Medigenomix for performance of the microsatellite linkage analysis, Elfi Holupirek and Kateryna Micklich for clinical-chemical analyses carried out at the GMC and the mouse facility of the Moorversuchsgut for excellent animal care.

Conflict of Interest statement. None declared.

FUNDING

This work was supported by the German Research Foundation (DFG) (grant number KE1673/1-1) and the National Genome Research Network (NGFN-Plus, grant numbers 01GS0850, 01GS0851 and Infrafrontier, grant number 01KX1012).

REFERENCES

1. Hart, T.C., Gorry, M.C., Hart, P.S., Woodard, A.S., Shihabi, Z., Sandhu, J., Shirts, B., Xu, L., Zhu, H., Barmada, M.M. *et al.* (2002) Mutations of the UMOD gene are responsible for medullary cystic kidney disease 2 and familial juvenile hyperuricaemic nephropathy. *J. Med. Genet.*, **39**, 882–892.
2. Scolari, F., Caridi, G., Rampoldi, L., Tardanico, R., Izzi, C., Pirulli, D., Amoroso, A., Casari, G. and Ghiggeri, G.M. (2004) Uromodulin storage diseases: clinical aspects and mechanisms. *Am. J. Kidney Dis.*, **44**, 987–999.
3. Zaucke, F., Boehnlein, J.M., Steffens, S., Polishchuk, R.S., Rampoldi, L., Fischer, A., Pasch, A., Boehm, C.W., Baasner, A., Attanasio, M. *et al.* (2010) Uromodulin is expressed in renal primary cilia and UMOD mutations result in decreased ciliary uromodulin expression. *Hum. Mol. Genet.*, **19**, 1985–1997.
4. Rampoldi, L., Scolari, F., Amoroso, A., Ghiggeri, G. and Devuyst, O. (2011) The rediscovery of uromodulin (Tamm-Horsfall protein): from tubulointerstitial nephropathy to chronic kidney disease. *Kidney Int.*, **80**, 338–347.
5. Bollee, G., Dahan, K., Flamant, M., Moriniere, V., Pawtowski, A., Heidet, L., Lacombe, D., Devuyst, O., Pirson, Y., Antignac, C. *et al.* (2011) Phenotype and outcome in hereditary tubulointerstitial nephritis secondary to UMOD mutations. *Clin. J. Am. Soc. Nephrol.*, **6**, 2429–2438.
6. Rampoldi, L., Caridi, G., Santon, D., Boaretto, F., Bernascone, I., Lamorte, G., Tardanico, R., Dagnino, M., Colussi, G., Scolari, F. *et al.* (2003) Allelism of MCKD, FJHN and GCKD caused by impairment of uromodulin export dynamics. *Hum. Mol. Genet.*, **12**, 3369–3384.
7. Bleyer, A.J., Zivna, M. and Kmoch, S. (2011) Uromodulin-associated kidney disease. *Nephron Clin. Pract.*, **118**, c31–c36.
8. Nasr, S.H., Lucia, J.P., Galgano, S.J., Markowitz, G.S. and D'Agati, V.D. (2008) Uromodulin storage disease. *Kidney Int.*, **73**, 971–976.
9. Vylet'al, P., Kublova, M., Kalbacova, M., Hodanova, K., Baresova, V., Stiburkova, B., Sikora, J., Hulkova, H., Zivny, J., Majewski, J. *et al.* (2006) Alterations of uromodulin biology: a common denominator of the genetically heterogeneous FJHN/MCKD syndrome. *Kidney Int.*, **70**, 1155–1169.
10. Smith, G.D., Robinson, C., Stewart, A.P., Edwards, E.L., Karet, H.I., Norden, A.G., Sandford, R.N. and Karet Frankl, F.E. (2011) Characterization of a recurrent in-frame UMOD indel mutation causing late-onset autosomal dominant end-stage renal failure. *Clin. J. Am. Soc. Nephrol.*, **6**, 2766–2774.
11. Williams, S.E., Reed, A.A., Galvanovskis, J., Antignac, C., Goodship, T., Karet, F.E., Kotanko, P., Lhotta, K., Moriniere, V., Williams, P. *et al.* (2009) Uromodulin mutations causing familial juvenile hyperuricaemic

nephropathy lead to protein maturation defects and retention in the endoplasmic reticulum. *Hum. Mol. Genet.*, **18**, 2963–2974.
12. Tamm, I. and Horsfall, F.L. Jr. (1950) Characterization and separation of an inhibitor of viral hemagglutination present in urine. *Proc. Soc. Exp. Biol. Med.*, **74**, 106–108.
13. Pennica, D., Kohr, W.J., Kuang, W.J., Glaister, D., Aggarwal, B.B., Chen, E.Y. and Goeddel, D.V. (1987) Identification of human uromodulin as the Tamm-Horsfall urinary glycoprotein. *Science*, **236**, 83–88.
14. Hoyer, J.R., Sisson, S.P. and Vernier, R.L. (1979) Tamm-Horsfall glycoprotein: ultrastructural immunoperoxidase localization in rat kidney. *Lab. Invest.*, **41**, 168–173.
15. Van Rooijen, J.J., Voskamp, A.F., Kamerling, J.P. and Vliegenthart, J.F. (1999) Glycosylation sites and site-specific glycosylation in human Tamm-Horsfall glycoprotein. *Glycobiology*, **9**, 21–30.
16. Serafini-Cessi, F., Malagolini, N. and Cavallone, D. (2003) Tamm-Horsfall glycoprotein: biology and clinical relevance. *Am. J. Kidney Dis.*, **42**, 658–676.
17. Bachmann, S., Mutig, K., Bates, J., Welker, P., Geist, B., Gross, V., Luft, F.C., Alenina, N., Bader, M., Thiele, B.J. *et al.* (2005) Renal effects of Tamm-Horsfall protein (uromodulin) deficiency in mice. *Am. J. Physiol. Renal Physiol.*, **288**, F559–F567.
18. Raffi, H., Bates, J.M., Laszik, Z. and Kumar, S. (2006) Tamm-Horsfall protein knockout mice do not develop medullary cystic kidney disease. *Kidney Int.*, **69**, 1914–1915.
19. Bernascone, I., Vavassori, S., Di Pentima, A., Santambrogio, S., Lamorte, G., Amoroso, A., Scolari, F., Ghiggeri, G.M., Casari, G., Polishchuk, R. *et al.* (2006) Defective intracellular trafficking of uromodulin mutant isoforms. *Traffic*, **7**, 1567–1579.
20. Kemter, E., Rathkolb, B., Rozman, J., Hans, W., Schrewe, A., Landbrecht, C., Klaften, M., Ivandic, B., Fuchs, H., Gailus-Durner, V. *et al.* (2009) Novel missense mutation of uromodulin in mice causes renal dysfunction with alterations in urea handling, energy, and bone metabolism. *Am. J. Physiol. Renal Physiol.*, **297**, F1391–F1398.
21. Kottgen, A., Pattaro, C., Boger, C.A., Fuchsberger, C., Olden, M., Glazer, N.L., Parsa, A., Gao, X., Yang, Q., Smith, A.V. *et al.* (2010) New loci associated with kidney function and chronic kidney disease. *Nat. Genet.*, **42**, 376–384.
22. Gudbjartsson, D.F., Holm, H., Indridason, O.S., Thorleifsson, G., Edvardsson, V., Sulem, P., de Vegt, F., d'Ancona, F.C., den Heijer, M., Wetzels, J.F. *et al.* (2010) Association of variants at UMOD with chronic kidney disease and kidney stones-role of age and comorbid diseases. *PLoS genetics*, **6**, e1001039.
23. Kottgen, A., Glazer, N.L., Dehghan, A., Hwang, S.J., Katz, R., Li, M., Yang, Q., Gudnason, V., Launer, L.J., Harris, T.B. *et al.* (2009) Multiple loci associated with indices of renal function and chronic kidney disease. *Nat. Genet.*, **41**, 712–717.
24. Han, J., Liu, Y., Rao, F., Nievergelt, C.M., O'Connor, D.T., Wang, X., Liu, L., Bu, D., Liang, Y., Wang, F. *et al.* (2013) Common genetic variants of the human uromodulin gene regulate transcription and predict plasma uric acid levels. *Kidney Int.*, **83**, 733–740.
25. Aigner, B., Rathkolb, B., Herbach, N., Kemter, E., Schessl, C., Klaften, M., Klempt, M., Hrabe de Angelis, M., Wanke, R. and Wolf, E. (2007) Screening for increased plasma urea levels in a large-scale ENU mouse mutagenesis project reveals kidney disease models. *Am. J. Physiol. Renal Physiol.*, **292**, F1560–F1567.
26. Keays, D.A., Clark, T.G., Campbell, T.G., Broxholme, J. and Valdar, W. (2007) Estimating the number of coding mutations in genotypic and phenotypic driven N-ethyl-N-nitrosourea (ENU) screens: revisited. *Mamm. Genome*, **18**, 123–124.
27. Yang, B. and Bankir, L. (2005) Urea and urine concentrating ability: new insights from studies in mice. *Am. J. Physiol. Renal Physiol.*, **288**, F881–F896.
28. Martensson, J., Martling, C.R. and Bell, M. (2012) Novel biomarkers of acute kidney injury and failure: clinical applicability. *Br. J. Anaesth.*, **109**, 843–850.
29. Gillece, P., Luz, J.M., Lennarz, W.J., de La Cruz, F.J. and Romisch, K. (1999) Export of a cysteine-free misfolded secretory protein from the endoplasmic reticulum for degradation requires interaction with protein disulfide isomerase. *J. Cell. Biol.*, **147**, 1443–1456.
30. Inagi, R. (2009) Endoplasmic reticulum stress in the kidney as a novel mediator of kidney injury. *Nephron Exp. Nephrol.*, **112**, e1–e9.
31. Guerriero, C.J. and Brodsky, J.L. (2012) The delicate balance between secreted protein folding and endoplasmic reticulum-associated degradation in human physiology. *Physiol. Rev.*, **92**, 537–576.
32. Vembar, S.S. and Brodsky, J.L. (2008) One step at a time: endoplasmic reticulum-associated degradation. *Nat. Rev. Mol. Cell Biol.*, **9**, 944–957.
33. Jennings, P., Aydin, S., Kotanko, P., Lechner, J., Lhotta, K., Williams, S., Thakker, R.V. and Pfaller, W. (2007) Membrane targeting and secretion of mutant uromodulin in familial juvenile hyperuricemic nephropathy. *J. Am. Soc. Nephrol.*, **18**, 264–273.
34. Bleyer, A.J., Hart, T.C., Shihabi, Z., Robins, V. and Hoyer, J.R. (2004) Mutations in the uromodulin gene decrease urinary excretion of Tamm-Horsfall protein. *Kidney Int.*, **66**, 974–977.
35. Wolf, M.T., Beck, B.B., Zaucke, F., Kunze, A., Misselwitz, J., Ruley, J., Ronda, T., Fischer, A., Eifinger, F., Licht, C. *et al.* (2007) The Uromodulin C744G mutation causes MCKD2 and FJHN in children and adults and may be due to a possible founder effect. *Kidney Int.*, **71**, 574–581.
36. Waldherr, R., Lennert, T., Weber, H.P., Fodisch, H.J. and Scharer, K. (1982) The nephronophthisis complex. A clinicopathologic study in children. *Virchows Arch. A. Pathol. Anat. Histol.*, **394**, 235–254.
37. Gusmano, R., Caridi, G., Marini, M., Perfumo, F., Ghiggeri, G.M., Piaggio, G., Ceccherini, I. and Seri, M. (2002) Glomerulocystic kidney disease in a family. *Nephrol. Dial. Transplant.*, **17**, 813–818.
38. Wolf, M.T., Mucha, B.E., Attanasio, M., Zalewski, I., Karle, S.M., Neumann, H.P., Rahman, N., Bader, B., Baldamus, C.A., Otto, E. *et al.* (2003) Mutations of the Uromodulin gene in MCKD type 2 patients cluster in exon 4, which encodes three EGF-like domains. *Kidney Int.*, **64**, 1580–1587.
39. Dahan, K., Devuyst, O., Smaers, M., Vertommen, D., Loute, G., Poux, J.M., Viron, B., Jacquot, C., Gagnadoux, M.F., Chauveau, D. *et al.* (2003) A cluster of mutations in the UMOD gene causes familial juvenile hyperuricemic nephropathy with abnormal expression of uromodulin. *J. Am. Soc. Nephrol.*, **14**, 2883–2893.
40. Benetti, E., Caridi, G., Vella, M.D., Rampoldi, L., Ghiggeri, G.M., Artifoni, L. and Murer, L. (2009) Immature renal structures associated with a novel UMOD sequence variant. *Am. J. Kidney Dis.*, **53**, 327–331.
41. Kimura, K., Jin, H., Ogawa, M. and Aoe, T. (2008) Dysfunction of the ER chaperone BiP accelerates the renal tubular injury. *Biochem. Biophys. Res. Commun.*, **366**, 1048–1053.
42. Prunotto, M., Budd, D.C., Gabbiani, G., Meier, M., Formentini, I., Hartmann, G., Pomposiello, S. and Moll, S. (2012) Epithelial-mesenchymal crosstalk alteration in kidney fibrosis. *J. Pathol.*, **228**, 131–147.
43. Bohle, A., Mackensen-Haen, S. and von Gise, H. (1987) Significance of tubulointerstitial changes in the renal cortex for the excretory function and concentration ability of the kidney: a morphometric contribution. *Am. J. Nephrol.*, **7**, 421–433.
44. Choi, H.K., Mount, D.B. and Reginato, A.M. (2005) Pathogenesis of gout. *Ann. Intern. Med.*, **143**, 499–516.
45. Rezende-Lima, W., Parreira, K.S., Garcia-Gonzalez, M., Riveira, E., Banet, J.F. and Lens, X.M. (2004) Homozygosity for uromodulin disorders: FJHN and MCKD-type 2. *Kidney Int.*, **66**, 558–563.
46. Takiue, Y., Hosoyamada, M., Yokoo, T., Kimura, M., Ochiai, M., Kaneko, K., Ichida, K., Hosoya, T. and Shibasaki, T. (2008) Production and characterization of transgenic mice harboring mutant human UMOD gene. *Nucleosides Nucleotides Nucleic Acids*, **27**, 596–600.
47. Bernascone, I., Janas, S., Ikehata, M., Trudu, M., Corbelli, A., Schaeffer, C., Rastaldi, M.P., Devuyst, O. and Rampoldi, L. (2010) A transgenic mouse model for uromodulin-associated kidney diseases shows specific tubulo-interstitial damage, urinary concentrating defect and renal failure. *Hum. Mol. Genet.*, **19**, 2998–3010.
48. Rathkolb, B., Decker, T., Fuchs, E., Soewarto, D., Fella, C., Heffner, S., Pargent, W., Wanke, R., Balling, R., Hrabe de Angelis, M. *et al.* (2000) The clinical-chemical screen in the Munich ENU Mouse Mutagenesis Project: screening for clinically relevant phenotypes. *Mamm. Genome*, **11**, 543–546.
49. Gailus-Durner, V., Fuchs, H., Adler, T., Aguilar Pimentel, A., Becker, L., Bolle, I., Calzada-Wack, J., Dalke, C., Ehrhardt, N., Ferwagner, B. *et al.* (2009) Systemic first-line phenotyping. *Methods Mol. Biol.*, **530**, 463–509.
50. Liu, Y., El-Achkar, T.M. and Wu, X.R. (2012) Tamm-Horsfall protein regulates circulating and renal cytokines by affecting glomerular filtration rate and acting as a urinary cytokine trap. *J. Biol. Chem*, **287**, 16365–16378.
51. Kemter, E., Rathkolb, B., Bankir, L., Schrewe, A., Hans, W., Landbrecht, C., Klaften, M., Ivandic, B., Fuchs, H., Gailus-Durner, V. *et al.* (2010) Mutation of the Na+-K+-2Cl- cotransporter NKCC2 in mice is associated with severe polyuria and a urea-selective concentrating defect without hyperreninemia. *Am. J. Physiol. Renal Physiol.*, **298**, F1405–F1415.

52. Weibel, E.R. (1979) *Stereological Methods. I. Practical Methods for Biological Morphometry*. Academic Press, London.
53. Klose, R., Kemter, E., Bedke, T., Bittmann, I., Kelsser, B., Endres, R., Pfeffer, K., Schwinzer, R. and Wolf, E. (2005) Expression of biologically active human TRAIL in transgenic pigs. *Transplantation*, **80**, 222–230.
54. Schaffer, P., Gombos, E., Meichelbeck, K., Kiss, A., Hart, P.S. and Bleyer, A.J. (2010) Childhood course of renal insufficiency in a family with a uromodulin gene mutation. *Pediatr. Nephrol.*, **25**, 1355–1360.
55. Bleyer, A.J., Trachtman, H., Sandhu, J., Gorry, M.C. and Hart, T.C. (2003) Renal manifestations of a mutation in the uromodulin (Tamm Horsfall protein) gene. *Am. J. Kidney Dis.*, **42**, E20–E26.